BIOLOGICAL CRYSTALLOGRAPHY
ISSN 1399-0047

Insights into stabilizing interactions in the distorted domain-swapped dimer of *Salmonella typhimurium* survival protein

Yamuna Kalyani Mathiharan,[a] H. S. Savithri[b] and M. R. N. Murthy[a]*

[a]Molecular Biophysics Unit, Indian Institute of Science, Bangalore 560 012, India, and [b]Department of Biochemistry, Indian Institute of Science, Bangalore 560 012, India. *Correspondence e-mail: mrn@mbu.iisc.ernet.in

Received 26 April 2015
Accepted 22 June 2015

Edited by K. Miki, Kyoto University, Japan

Keywords: SurE; domain swapping; oligomeric structure; symmetry; structure–function relationship.

PDB references: *St*SurE, E112A mutant, *F*222 form, 4ryt; *C*2 form, 4ryu; E112A mutant, soaked with AMP, 4xj7; E112A/H234A mutant, form I, 4xgb; form II, 4xgp; E112A/H234A mutant, *F*222 form, 4xep; *C*2 form, 4xer; E112A/D230A mutant, 4xh8

Supporting information: this article has supporting information at journals.iucr.org/d

The survival protein SurE from *Salmonella typhimurium* (*St*SurE) is a dimeric protein that functions as a phosphatase. SurE dimers are formed by the swapping of a loop with a pair of β-strands and a C-terminal helix between two protomers. In a previous study, the Asp230 and His234 residues were mutated to Ala to abolish a hydrogen bond that was thought to be crucial for C-terminal helix swapping. These mutations led to functionally inactive and distorted dimers in which the two protomers were related by a rotation of 167°. New salt bridges involving Glu112 were observed in the dimeric interface of the H234A and D230A/H234A mutants. To explore the role of these salt bridges in the stability of the distorted structure, E112A, E112A/D230A, E112A/H234A, E112A/D230A/H234A, R179L/H180A/H234A and E112A/R179L/H180A/H234A mutants were constructed. X-ray crystal structures of the E112A, E112A/H234A and E112A/D230A mutants could be determined. The dimeric structures of the E112A and E112A/H234A mutants were similar to that of native SurE, while the E112A/D230A mutant had a residual rotation of 11° between the *B* chains upon superposition of the *A* chains of the mutant and native dimers. The native dimeric structure was nearly restored in the E112A/H234A mutant, suggesting that the new salt bridge observed in the H234A and D230A/H234A mutants was indeed responsible for the stability of their distorted structures. Catalytic activity was also restored in these mutants, implying that appropriate dimeric organization is necessary for the activity of SurE.

1. Introduction

In several proteins, oligomerization appears to be the result of an exchange of identical domains between protomers. Random mutations in a hinge region connecting two spatial domains of a protomer may promote the swapping of domains. Equivalence of swapping interactions may ensure symmetry of the resulting oligomer. In the course of evolution, other interfaces of such symmetric oligomers might become stabilized by favourable mutations, and swapping may no longer be needed to maintain the symmetry and integrity of the oligomer (Ali & Imperiali, 2005). It is therefore of interest to understand the role of interfaces and hinge regions in domain swapping. We have selected the *Salmonella typhimurium* survival protein SurE (*St*SurE) as a model system for such studies.

SurE is one of several proteins that are expressed in bacteria in response to environmental stresses. X-ray crystal structures of SurE from *S. typhimurium* (*St*SurE; PDB entry 2v4n; Pappachan *et al.*, 2008), *Thermotoga maritima* (*Tm*SurE; PDB entry 1j9j; Lee *et al.*, 2001; Zhang *et al.*, 2001), *Thermus thermophilus* (*Tt*SurE; PDB entry 2e6e; Iwasaki & Miki, 2007), *Aquifex aeolicus* (*Aa*SurE; PDB entry 2wqk; Antonyuk

et al., 2009), *Pyrobaculum aerophilum* (*Pa*SurE; PDB entry 1l5x; Mura *et al.*, 2003), *Coxiella burnetii* (*Cb*SurE; PDB entry 3ty2; Franklin *et al.*, 2015) and *Brucella abortus* (*Ba*SurE; PDB entry 4zgs; K. F. Tarique, S. A. Abdul Rehman, S. Devi & S. Gourinath, unpublished work) have been determined. SurE has a Rossmann fold-like topology and functions as a divalent metal ion-dependent phosphatase specific to nucleotide monophosphates (Proudfoot *et al.*, 2004; Zhang *et al.*, 2001). SurEs appear to be dimeric or tetrameric in solution. *St*SurE is a dimer in solution, while in the crystal structure the dimers

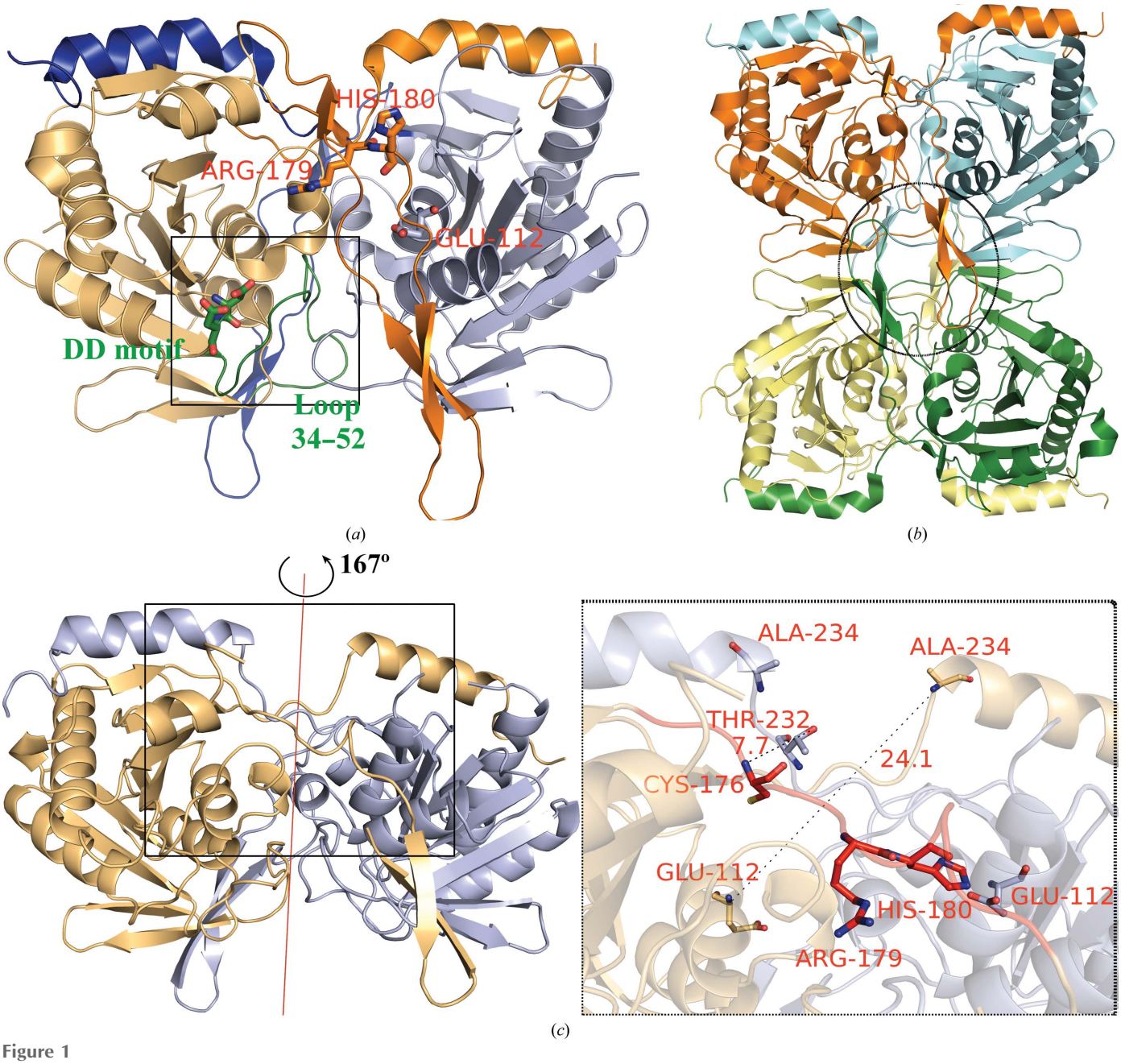

Figure 1
(*a*) Ribbon diagram of the *St*SurE dimer. The two protomers are coloured orange and blue, respectively. The exchanged domains of each protomer are represented in darker shades. The active site of protomer *A* (orange) is shown in a box. Within the box the DD motif (residues 8 and 9, ball-and-stick representation) and loop 34–52 are highlighted in green. Arg179^{A}, His180^{A} and Glu112^{B} are shown in ball-and-stick representation. These are the residues that are mutated in the present study. (*b*) Ribbon diagram of the tetrameric organization observed in *St*SurE and several of its homologues. Domain-swapped tetramerization loops from chains *A* (orange) and *C* (green) and chains *B* (blue) and *D* (yellow) are circled. (*c*) Distorted dimeric structure of H234A *St*SurE. The *A* (orange) and *B* (blue) chains are related by a rotation of 167°. The axis of rotation is shown as a red line. A similar dimeric organization is also found in the D230A/H234A mutant. The insert shows the hinge region where the H234A and D230A mutations were introduced and the location of residue Glu112 was targeted for further mutation. The distance between the C$^{\alpha}$ atoms of Glu112 (ball-and-stick representation) and Ala234 (ball-and-stick representation) in chain *A* of the H234A mutant is 24.1 Å. A similar distance was also observed between the C$^{\alpha}$ atoms of Glu112 and Ala234 in the *B* chain. The inset shows the loss of hydrogen bonds between Cys176^{A} and Thr232^{B}, which has affected the conformation of loop 174–184^{A} (dark orange) and has brought residues Arg179^{A} and His180^{A} closer to Glu112^{B}.

Table 1
Data-processing and refinement statistics.

The unit-cell parameters of native *St*SurE in the *C*2 form are $a = 161.1$, $b = 95.3$, $c = 94.6$ Å, $\alpha = 90$, $\beta = 98.9$, $\gamma = 90^\circ$ and those in the *F*222 form are $a = 73.7$, $b = 121.6$, $c = 143.3$ Å, $\alpha = 90$, $\beta = 90$, $\gamma = 90^\circ$.

	E112A		E112A/H234A					
	*C*2	*F*222	*C*2	*F*222	E112A/D230A	E112A soaked with AMP	E112A/H234A co-crystallized with AMP, form I	E112A/H234A co-crystallized and soaked with AMP, form II
Unit-cell parameters								
a (Å)	160.4	73.0	165.6	73.5	92.3	160.6	161.4	162.5
b (Å)	95.8	121.2	96.5	121.7	92.3	95.8	96.5	96.2
c (Å)	94.2	143.8	95.0	143.4	150.4	94.8	94.5	93.9
$\alpha = \gamma$ (°)	90	90	90	90	90	90	90	90
β (°)	100.1	90	98.6	90	90	100.1	99.3	98.4
Space group	*C*2	*F*222	*C*2	*F*222	$P4_12_12$	*C*2	*C*2	*C*2
Resolution (Å)	47.87–2.03 (2.14–2.03)	46.33–2.07 (2.18–2.07)	40.32–1.97 (2.07–1.97)	50.00–1.50 (1.53–1.50)	49.30–3.56 (3.90–3.56)	24.89–1.60 (1.69–1.60)	59.38–2.21 (2.33–2.21)	32.87–1.90 (2.00–1.90)
Total No. of reflections	352139	90888	444369	474013	28198	729896	175750	380936
No. of unique reflections	89024 (11902)	18453 (2258)	104677 (15172)	49090 (1932)	6585 (1550)	184243 (26589)	67404 (7850)	111344 (16131)
Multiplicity	4.0 (3.5)	4.9 (4.6)	4.2 (4.1)	9.7 (4.1)	4.3 (2.9)	4.0 (3.8)	2.6 (2.3)	3.4 (3.4)
Mean $I/\sigma(I)$	11.5 (2.3)	12.6 (5.7)	14.2 (2.6)	68.1 (2.4)	4.9 (1.8)	12.1 (1.8)	6.3 (2.6)	8.9 (1.9)
R_{merge}† (%)	8.5 (53.4)	11.2 (19.7)	5.7 (49.8)	7.4 (47.9)	19.3 (56.0)	5.4 (59.5)	13.3 (35.6)	7.0 (62.4)
Completeness (%)	98.6 (91.0)	94.0 (79.6)	99.9 (99.5)	95.5 (75.4)	81.2 (82.4)	99.2 (98.3)	94.6 (75.6)	99.0 (98.4)
Protomers in asymmetric unit	4	1	4	1	2	4	4	4
Solvent content (%)	60.7	56.0	62.6	56.3	56.3	60.9	61.4	61.4
Refinement statistics								
R_{work}‡ (%)	17.81	20.34	16.52	18.71	26.18	17.50	20.82	18.90
R_{free}‡ (%)	21.42	24.44	21.39	22.86	30.42	20.80	26.25	23.98
R.m.s.d. from ideal values								
Bond angles (°)	1.37	1.29	1.80	1.89	0.92	1.66	1.20	1.77
Bond lengths (Å)	0.007	0.006	0.017	0.014	0.005	0.012	0.006	0.015
No. of atoms								
Protein	7708	1928	7752	2137	3477	7895	7716	7740
Water	933	289	878	353	23	1385	821	991
Ligands/ions	108	27	26	22	—	90	27	39
Mean *B* factors (Å^2)								
Protein	31.3	30.2	39.5	30.3	80.5	23.6	25.0	41.1
Water	43.3	43.9	50.8	47.4	44.4	40.6	28.4	50.0
Ligands/ions	49.0	41.8	54.8	52.2	—	39.1	25.9	58.4
Residues in Ramachandran plot (%)								
Favoured region	89.74	89.60	90.08	89.40	86.40	89.00	89.10	88.30
Allowed region	10.02	10.40	9.45	10.10	13.10	10.8	10.40	11.30
Generously allowed region	0.24	0.00	0.47	0.50	0.50	0.20	0.50	0.40
Disallowed region	0.00	0.00	0.00	0.00	0.00	0.00	0.00	0.00
PDB code	4ryu	4ryt	4xer	4xep	4xh8	4xj7	4xgb	4xgp

† $R_{merge} = \sum_{hkl}\sum_i |I_i(hkl) - \langle I(hkl)\rangle| / \sum_{hkl}\sum_i I_i(hkl)$, where $I_i(hkl)$ is the ith observation of reflection hkl and $\langle I(hkl)\rangle$ is its mean intensity. ‡ $R_{work} = \sum_{hkl} ||F_{obs}| - |F_{calc}|| / \sum_{hkl} |F_{obs}|$, R_{free} was calculated similarly using 5% of the reflections, which were excluded from refinement.

(Fig. 1*a*) associate to form a loose tetramer (Pappachan *et al.*, 2008; Fig. 1*b*). The *St*SurE structure was determined in two crystal forms: one in the orthorhombic space group *F*222 containing one protomer in the asymmetric unit and the other in a monoclinic *C*2 form with four protomers in the asymmetric unit (Pappachan *et al.*, 2008). In both forms of *St*SurE, as well as in all homologues, a similar tetrameric organization of protomers is observed.

Dimers of all SurE homologues have a swapped 'tetramerization loop' comprised of a pair of β-strands (Fig. 1*a*) that are involved in the formation of a loose tetramer (Fig. 1*b*). In addition to this, there is another helical segment at the C-terminus that is swapped between the protomers (Fig. 1*a*) in all homologues except for *Pa*SurE (Mura *et al.*, 2003). Structure and sequence comparison of the hinge regions of *St*SurE and *Pa*SurE involved in C-terminal helix swapping suggested that the intrachain hydrogen bond Asp230 OD2–His234 NE2 (2.89 Å) in *St*SurE might be crucial for domain swapping (Mathiharan *et al.*, 2013). Mutation of Asp230 and His234 resulted in dramatic changes in the dimeric organization, although the C-terminal helix swapping was mostly conserved (Mathiharan *et al.*, 2013). The two protomers of the distorted dimer were related by a rotation of 167° (Fig. 1*c*) and the dimers were functionally inactive (Mathiharan *et al.*, 2013). The dimeric interface of these mutants appeared to be stabilized by new salt bridges involving residue Glu112, which is ~24 Å away from the hinge (Fig. 1*c*). In order to explore the importance of these salt bridges, E112A, E112A/D230A, E112A/H234A, E112A/D230A/H234A, R179L/H180A/H234A and E112A/R179L/H180A/H234A mutants were constructed. Surprisingly, the native dimeric structure was restored in several of these mutants. The results of this study underscore the complexity of protein folding and association and suggest that predicting mutational effects is likely to

remain difficult, particularly when they involve residues that are crucial for domain swapping. These studies also have implications for the mechanism of evolution of symmetric protein oligomers.

2. Materials and methods

2.1. Cloning, overexpression and purification of the mutants

*St*SurE H234A, D230A and D230A/H234A mutants were cloned in Invitrogen pRSETC vector (Mathiharan *et al.*, 2013; Pappachan *et al.*, 2008). Mutants were constructed by site-directed mutagenesis (SDM). The template and primers used for PCR amplification and the restriction enzymes used for screening of the E112A, E112A/D230A, E112A/H234A, E112A/D230A/H234A, R179L/H180A/H234A and E112A/R179L/H180A/H234A mutants are given in Supplementary Table S1. The mutants were screened by digestion with the respective restriction enzymes. The mutations were further confirmed by DNA sequencing. The mutants were transformed into *Escherichia coli* BL21 pLysS cells. The protocols used for the overexpression and purification of these mutants were similar to those used for the D230A, H234A and D230A/H234A *St*SurE mutants (Mathiharan *et al.*, 2013).

2.2. Biophysical characterization of the mutants

The oligomeric state of the proteins (1.7 mg ml^{-1}, 150 µl) was examined by gel-filtration chromatography on a S200 analytical column with a bed volume of 24 ml. Circular-dichroism (CD) spectra of *St*SurE and its mutants were recorded using a Jasco J715 spectropolarimeter. Protein (0.3 mg ml^{-1}) in 5 m*M* HEPES pH 7.5 was used in a cell with a path length of 1 mm to record the data every 0.5 nm with a response time of 4 s and a bandwidth of 2 nm. The T_m of the mutants was estimated by a thermal shift assay using SYPRO Orange dye. The concentration of the proteins in 5 m*M* HEPES pH 7.5 used in these experiments varied from 0.1 to 0.2 mg ml^{-1}.

2.3. Crystallization, data collection and processing

The E112A mutant could be crystallized in *C*2 and *F*222 forms by the microbatch method using a condition consisting of 0.2 *M* sodium citrate tribasic dihydrate, 0.1 *M* HEPES pH 7.5, 30% 2-methyl-2,4-pentanediol (MPD). Similar *C*2 and *F*222 forms of the E112A/H234A mutant could be obtained by the microbatch-under-oil method in conditions consisting of 0.02 *M* $CaCl_2$, 0.1 *M* sodium acetate pH 4.6, 30% MPD and of 0.02 *M* $MgCl_2$, 0.1 *M* HEPES pH 7.5, 22% polyacrylic acid sodium salt 5100, respectively. The E112A/D230A mutant was crystallized by the hanging-drop method in a crystallization condition consisting of 0.08 *M* $MgCl_2$, 0.1 *M* HEPES pH 7.5, 15% polyacrylic acid sodium salt. Trials to obtain AMP-bound crystals were carried out either by soaking or by co-crystallization. E112A mutant crystals were soaked in the crystallization condition containing 35 m*M* AMP and 30% glycerol as a cryoprotectant. E112A/H234A mutant crystals were either soaked or co-crystallized with 30–50 m*M* AMP. X-ray diffraction data were collected from these crystals at 100 K as described in a previous publication (Mathiharan *et al.*, 2013). The data-processing statistics are listed in Table 1.

2.4. Structure determination, validation and analysis

The structures of mutants were determined by molecular replacement (MR) using *Phaser* (McCoy *et al.*, 2007). The structures were refined with *REFMAC* (Murshudov *et al.*, 2011) from the *CCP*4 suite (Winn *et al.*, 2011). The resulting structures were examined and manually built using *Coot* (Emsley *et al.*, 2010). Water molecules were identified using *REFMAC* and by manual examination of difference electron-density maps. Final models obtained after alternative cycles of model building and refinement were validated using *PROCHECK* (Laskowski *et al.*, 1993). Average *B* factors were calculated using the *BAVERAGE* program in the *CCP*4 suite (Winn *et al.*, 2011). Structural alignments were obtained using *ALIGN* (Cohen, 1997) and the SSM Superpose option of *Coot* (Krissinel & Henrick, 2004). Illustrations of structures were produced using *PyMOL* (v.1.5.0.4; Schrödinger). The channel volume was calculated using the *CASTp* server (Liang *et al.*, 1998*a*,*b*).

2.5. Alkaline phosphatase assay

The protein used in the assay was first dialyzed against a buffer consisting of 50 m*M* Tris pH 8, 100 m*M* NaCl, 10 m*M* EDTA. The reaction mixture (500 µl) consisted of 0–100 m*M* *p*-nitrophenyl phosphate (pNPP), 100 m*M* cacodylate pH 7, 10 m*M* $MgCl_2$ and 720–100 µg protein. The concentration of protein was estimated by measurement of the OD at 280 nm. The reaction mixture without the protein was used as a blank. After addition of the protein, the yellow-coloured *p*-nitrophenol product formed during the reaction was estimated by recording the OD at 405 nm for 5–20 min at 25°C. The slope of the curve was estimated to determine the change in OD per minute. The enzyme activity (V) at various substrate concentrations was calculated and plotted against the substrate concentration. The curve was fitted with Michaelis–Menten or positive cooperative kinetics using *GraphPad Prism* v.5.01 for Windows (GraphPad Software) and kinetic parameters were calculated. The equation used to calculate kinetic parameters in the case of a reaction following Michaelis–Menten kinetics is

$$V = (V_{max}S)/(K_m + S), \quad (1)$$

where V_{max} (in µmol min^{-1} mg^{-1}) is the maximal velocity observed when all of the enzyme is present as enzyme–substrate complex, S (in m*M*) is the substrate concentration and K_m (in m*M*) is the Michaelis–Menten constant. The equation used to calculate kinetic parameters in the case of catalysis with cooperativity is the Hill equation,

$$V = (V_{max}[S]^h)/(K' + [S]^h), \quad (2)$$

where h is the Hill coefficient, [S] is the substrate concentration and $K' = ([S]_{0.5})^h$, where $[S]_{0.5}$ is the substrate concentration when $V = 0.5V_{max}$; therefore, $K' = K_m$ when $h = 1$.

3. Results

3.1. Rationale for selecting sites for mutation

In the *St*SurE dimer, the tetramerization loop (residues 185–200) and the C-terminal helix (residues 234–253) are anchored to the twofold related protomer by extensive interactions (Fig. 1*a*; Pappachan *et al.*, 2008). These interactions are responsible for the concerted movement of these segments with the neighbouring protomer, with loops 174–184 and 227–234 functioning as hinges. These hinges are in close proximity owing to interchain hydrogen bonds between Cys176 and Thr232′ (Cys176 N–Thr232′ OG1, 2.8 Å; Cys176 SG–Thr232′ OG1, 3.5 Å, where a prime denotes a residue from the neighbouring subunit) in the wild-type dimer (*A*/*B*). In the distorted H234A and D230A/H234A mutants, changes in the conformation of the hinge 227–234 led to the loss of hydrogen bonds between Cys176 and Thr232′ (Fig. 1*c*, insert). Therefore, the loop 174–184 also undergoes a conformational change. These structural rearrangements in the mutants reduce the distance between the interface residues Glu112, Arg179 and His180 (Fig. 1*c*, insert). The distances between the C^{α} atoms of Glu112^{A} (where the superscript denotes the chain) and Arg179^{B} in the native and the H234A mutant are ∼13 and 9 Å, respectively. Similarly, the distance between the C^{α} atoms of Glu112^{B} and His180^{A} in native *St*SurE and the H234A mutant are ∼12.5 and 10.6 Å, respectively. Apart from the shorter distance between these residues, the side chains of Arg179 and His180 undergo large changes in the hinge mutants and become oriented towards Glu112. As a consequence, new salt bridges Glu112^{A}–Arg179^{B} and His180^{A}–Glu112^{B} are formed in the H234A mutant. Similar salt bridges are also found in the D230A/H234A mutant.

In native *St*SurE, Glu112^{A} interacts with Tyr103^{B} (Glu112^{A} OE2–Tyr103^{B} OH, 2.6 Å; Fig. 2*a*) and similar interactions are formed by Glu112^{B} with Tyr103^{A}. In the H234A mutant, Glu112^{A} forms a salt bridge with Arg179^{B}, and Glu112^{B} forms a salt bridge with His180^{A} (Glu112^{A} OE1–Arg179^{B} NH2, 3.1 Å; Glu112^{A} OE1–Arg179^{B} NE, 3.5 Å; Glu112^{A} OE2–Arg179^{B} NE, 3.2 Å; Glu112^{B} OE2–His180^{A} NE2, 3.1 Å; Fig. 2*b*). Similarly, in the D230A/H234A mutant, Glu112^{A} forms a salt bridge with Arg179^{B} (Glu112^{A} OE1–Arg179^{B} NH2, 3.1 Å; Glu112^{A} OE2–Arg179^{B} NE, 3.1 Å; Fig. 2*c*). These salt bridges probably contribute to the stability of the distorted dimeric structures.

In order to explore the importance of the salt bridge between Glu112 and Arg179′ or His180′ in the mutants, Glu112 was mutated to Ala, while Arg179 and His180 were mutated to Leu and Ala, respectively. The E112A, E112A/D230A, E112A/H234A, E112A/D230A/H234A, R179L/H180A/H234A and E112A/R179L/H180A/H234A mutants were constructed by site-directed mutagenesis. These mutants are referred to as ‘salt-bridge mutants’.

3.2. Biophysical characterization of the mutants

The E112A, E112A/D230A, E112A/H234A, E112A/D230A/H234A, R179L/H180A/H234A and E112A/R179L/H180A/H234A mutants could be expressed in soluble form. The yields of these mutants were 10, 1.5, 6, 0.5, 6 and 6 mg, respectively, per litre of culture. The size (28.5 kDa) and purity of the mutant proteins were confirmed by SDS–PAGE and mass spectrometry. Gel-filtration studies suggested that the E112A, E112A/H234A, E112A/D230A and E112A/D230A/H234A mutants eluted around 14.1–14.4 ml (the same as the elution volume of the native protein; Supplementary Figs. S1*a*–S1*d*), suggesting that they were dimeric in solution. Although soluble, the R179L/H180A/H234A and E112A/R179L/H180A/H234A mutants eluted in the void volume (∼8.3 ml), indicating that the mutant proteins had aggregated (Supplementary Figs. S1*e* and S1*f*). The CD spectra of the mutants had minima at 208 and 222 nm (Supplementary Fig. S2), as observed for wild-type *St*SurE, indicating that the mutants were well folded. Although the R179L/H180A/H234A and E112A/R179L/H180A/H234A mutants eluted in

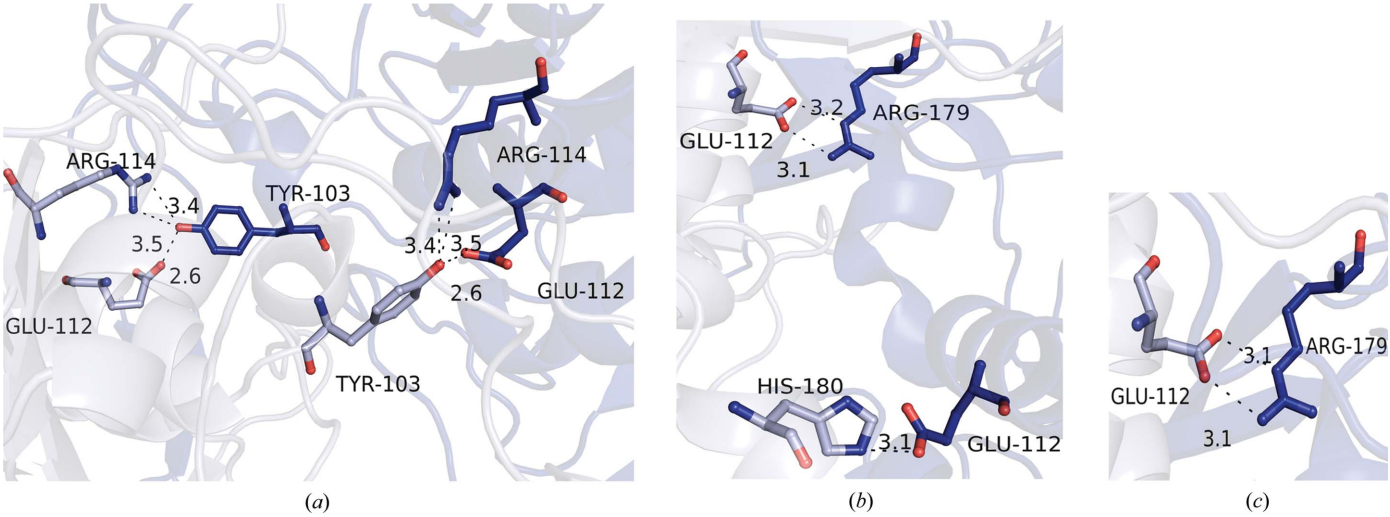

(*a*) (*b*) (*c*)

Figure 2
Interactions of the dimeric interface residue Glu112 in (*a*) native *St*SurE, (*b*) H234A *St*SurE and (*c*) D230A/H234A *St*SurE. The *A* and *B* chains are shown in light and dark shades of blue, respectively. The distances are in Å.

the void volume, their CD spectra exhibited minima at 208 and 222 nm, indicating that these mutants form soluble aggregates and that the structure of the protomer is probably retained.

Thermal denaturation profiles of the purified proteins were monitored by recording the fluorescence emitted by SYPRO Orange dye, which becomes bound to hydrophobic patches that are exposed upon protein unfolding. The T_m values of the native protein and the E112A, E112A/D230A, E112A/H234A and E112A/D230A/H234A mutants in HEPES buffer pH 7.5 were 41, 44, 41, 41 and 37°C (Supplementary Fig. S3), respectively, suggesting that all of these mutants are only moderately stable, although not significantly less stable than the wild-type protein.

3.3. Crystallization of mutant proteins and X-ray diffraction data collection

The E112A, E112A/H234A and E112A/D230A mutants were crystallized under the conditions given in §2. The E112A and E112A/H234A mutants crystallized in the monoclinic *C*2 and orthorhombic *F*222 space groups. These crystals were isomorphous to the corresponding native *St*SurE crystal forms. In the *C*2 form of the E112A/H234A mutant only, the *a* cell length was about 5 Å longer (Table 1). The isomorphism of the *F*222 form of the E112A/H234A mutant and native *St*SurE was completely unexpected, as the single-site mutant H234A had crystallized under similar conditions in space group $C222_1$ with unit-cell parameters that were unrelated to those of native *St*SurE. Thus, the introduction of an E112A mutation in addition to the H234A mutation appeared to have restored the crystal packing so that the space group and unit-cell parameters were similar to those of native *St*SurE. The E112A/D230A mutant crystallized in the tetragonal space group $P4_12_12$.

3.4. Determination of the structures of the mutants

The structures of the E112A, E112A/H234A and E112A/D230A mutants were determined by molecular replacement using *Phaser* (McCoy *et al.*, 2007). The search model used was an *St*SurE protomer from which residues 110–116 were excluded to avoid model bias. For the E112A/H234A and E112A/D230A mutants, residues 227–236 were also excluded from the search model. In all cases, a reasonable solution was

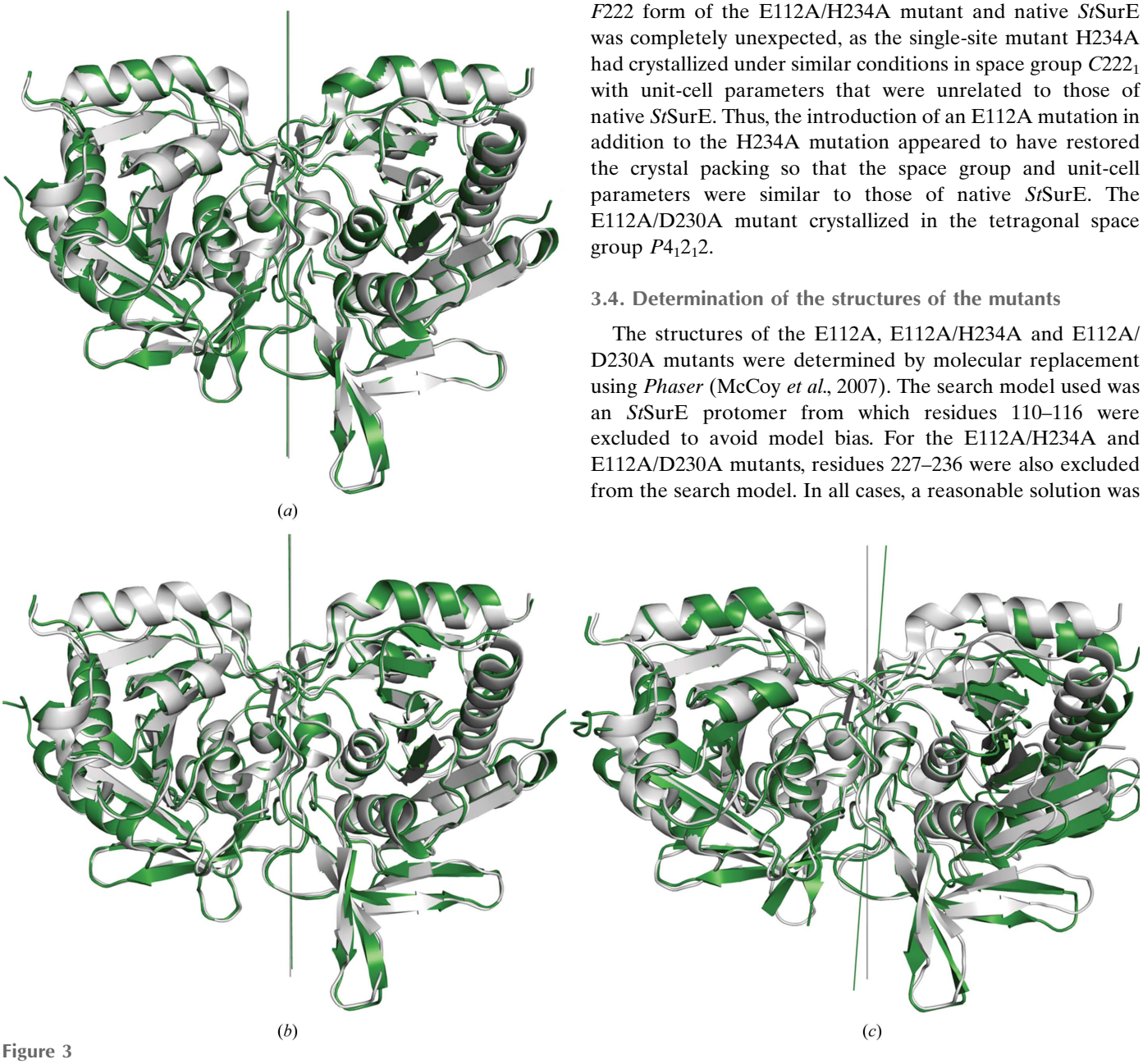

Figure 3
Comparison of the dimeric structure in wild-type and mutant *St*SurE. Superposition of wild-type (grey) and mutant (green) dimers was carried out using only the *A* chains for alignment. The rotation axes relating the *A*/*B* protomers in the native and the mutants are shown by grey and green lines, respectively. (*a*) E112A, (*b*) E112A/H234A. In both cases there was no residual rotation between the *B* chains and the rotation axes were nearly coincident. (*c*) In a comparison of the E112A/D230A mutant with the native structure, superposition of the *A* chains leads to an 11° difference in the orientation of the *B* subunits. The difference in the direction of the rotation axis relating the two subunits may be noted.

obtained. The ordered residues of the deleted segments were manually built using *Coot* (Emsley *et al.*, 2010) and the structures were refined by *REFMAC* (Murshudov *et al.*, 2011). The refinement statistics of the mutants are summarized in Table 1. R and $R_{\rm free}$ were only higher for the tetragonal form of the E112A/D230A mutant (26.2 and 30.4%, respectively), reflecting the low resolution and quality of the diffraction data. Examination of the structures using *PROCHECK* (Laskowski *et al.*, 1993) revealed that all of the residues are in the most allowed, allowed or generously allowed regions of the Ramachandran map.

3.5. Structure of the salt-bridge mutants

In all chains of the *F*222 and *C*2 forms of the E112A and E112A/H234A mutants, as expected, there was no difference density for the side chain of Glu112. Additionally, in the E112A/H234A mutant there was no difference density for the side chain of His234 either. In this mutant, the swapped conformation of the C-terminal helix fitted the difference density better than the unswapped conformation. In the E112A/D230A mutant, residues 227–234 that are involved in C-terminal helix swapping were disordered and the lower resolution of the data did not permit modelling of this region with confidence. However, the electron densities corresponding to the C-terminal helices as well as the segment surrounding the mutated residue 112 were significant.

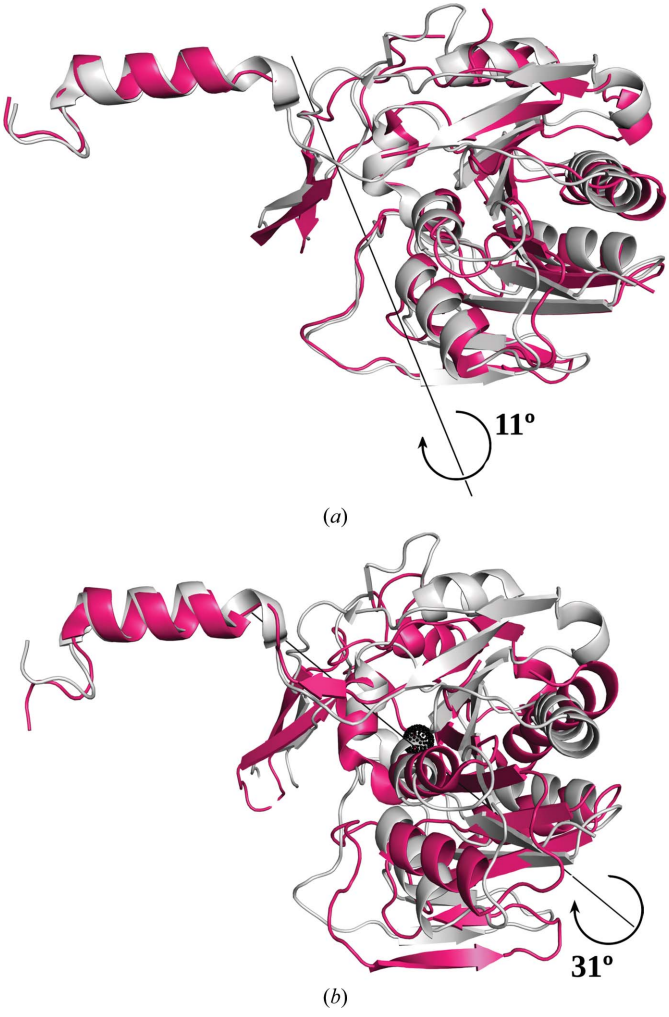

Figure 4
Rotation axes relating the *B* chains of native and mutant structures upon superposition of their *A* chains. (*a*) Axis about which an 11° residual rotation is observed between the E112A/D230A mutant (pink) and native (grey) *B* chains. (*b*) Axis about which a residual rotation of 31° is observed between the H234A mutant (pink) and native (grey) *B* chains. The black sphere marks the centroid of the *B* chain of native *St*SurE. The angle between the two axes is 46°.

Native *St*SurE is a symmetric dimer, while the H234A and D230A/H234A mutants are highly distorted dimers (Figs. 1*a* and 1*c*). Therefore, it was surprising that the two subunits were related by a rotation of ∼180° in the E112A/H234A and E112A/D230A mutants (Fig. 3), as in the native form. An equivalent dimeric organization was also found in the E112A mutant. To compare the dimeric organizations of these structures, chain *A* of the mutants was superposed on chain *A* of the native structure using the SSM Superpose tool in *Coot* (Krissinel & Henrick, 2004). This resulted in good superposition of the *B* chains in the E112A and E112A/H234A mutants (Figs. 3*a* and 3*b*). However, a similar superposition of the *A* chain of the E112A/D230A mutant resulted in a residual rotation of ∼11° between the *B* chains (Figs. 3*c* and 4*a*). The rotation axis relating the two protomers (*A*/*B*) in the E112A/D230A mutant is at a small angle of ∼4° from the rotation axis relating the protomers in the native structure (Fig. 3*c*). Thus, the additional mutations introduced have largely alleviated the distortion of the dimer caused by the original H234A mutation. This restoration is less complete in the E112A/D230A mutant.

The 11° residual rotation between the *B* chains of the native and the E112A/D230A mutant (Fig. 3*c*) remaining after superposition of their *A* chains is around an axis passing through the *A*/*B* dimer interface (Fig. 4*a*). This axis is distinct from the axis around which 31° residual rotation was observed between the *B* chains of the native and the H234A or D230A/H234A mutants (Fig. 4*b*) in a similar superposition of only the *A* chains. This rotation axis (31°) passes close to the centroid of the native protomer *B* (Fig. 4*b*). The angle between this axis and the axis around which residual rotation is observed in the E112A/D230A mutant is ∼46°.

In the E112A and E112A/H234A mutants, changes were observed in the side-chain conformations of Ile102, Tyr103 and His115. This might be owing to the loss of hydrogen bonding between Glu112 and Tyr103 (Fig. 2*a*). In the E112A/H234A mutant, the hinge residues 227–234 involved in C-terminal helix swapping had the same conformation as in the wild type except for slight perturbations near the site of mutation (residue 234). Additionally, there were also structural changes in loop 34–52 near the active site.

3.6. Effects of mutations on the flexibility of *St*SurE

The deviations of the *B* factors of backbone atoms from the mean *B* factor of the respective chain plotted against residue number are shown in Fig. 5. In the H234A, D230A/H234A and

E112A/D230A mutants, the deviations associated with residues 125–253 constituting the C-terminal half were generally larger than those of the N-terminal half (residues 1–125). Thus, the mutations appear to substantially increase the flexibility of the C-terminal half. The catalytic properties of the mutants discussed in a later section may be related to the increased flexibility of the C-terminal half.

3.7. X-ray diffraction data collection and structure determination of ligand-bound mutants

X-ray crystal structures of the E112A and E112A/H234A mutants soaked or co-crystallized with AMP were determined. Data-collection and processing statistics of these structures are listed in Table 1. The structures of soaked or co-crystallized E112A and E112A/H234A mutants were determined starting with the coordinates of the *C*2 form of the respective unliganded structures. However, before initiating refinement, all metals atoms, ligands and water molecules were deleted from the coordinate set to avoid model bias. The data-refinement statistics of these structures are listed in Table 1. These structures also had a similar dimeric organization as the respective unliganded structures.

3.8. Ligands/ions bound near the active site of salt-bridge mutants and their implications

The active site of SurE is defined by a DD motif (residues 8 and 9; Fig. 1*a*) and a bound Mg^{2+} ion (Pappachan *et al.*, 2008). In all mutants except for in chain *A* of the *C*2 form of the E112A/H234A mutant and in both chains of the E112A/D230A mutant, density appropriate for an Mg^{2+} ion was observed. In chain *A* of the *C*2 form of the E112A/H234A mutant the density was much stronger and probably corresponds to a bound Ca^{2+} ion, which was part of the crystallization cocktail. In the E112A/D230A mutant no significant density for a bound metal ion was observed. This is probably owing to the low resolution and quality of the map. The distorted mutants also bind a metal ion in a similar site.

Significant electron density for bound phosphate ions was observed in the *F*222 and *C*2 forms of native *St*SurE and the E112A and E112A/H234A mutants, although the crystallization conditions of these proteins did not include phosphate. In these structures, phosphate ions bind near the active site at one of the two sites designated site 1 and site 2 (Fig. 6). At site 1 the phosphate is coordinated to 11 atoms: Mg^{2+}, the OD1 and OD2 atoms of Asp8, the main-chain N atoms of Gly40 and Gly105, the hydroxyl O atoms of Ser104 and Thr106 and the ND2 and OD1 atoms of Asn92 and Asn96 (Pappachan *et al.*, 2008). At site 2 the P atom of the phosphate ion is ∼6 Å away from the Mg^{2+} ion. At this site phosphate ion is held mainly by hydrogen bonding to a water network and the side chain of Asn96 (Pappachan *et al.*, 2008). In the AMP-soaked E112A mutant crystal structure, the active sites of chains *A* and *D* had density suitable for an adenosine moiety and a phosphate ion (Fig. 6*b*), while chain *B* had density for an adenine moiety and a phosphate ion. In the E112A/H234A mutant form II crystal structure, an adenine moiety and a phosphate ion were also bound at the active site of chain *A*. In all of these chains, the phosphate ion was at site 1 and the adenine ring was at a site referred to hereafter as the 'adenine

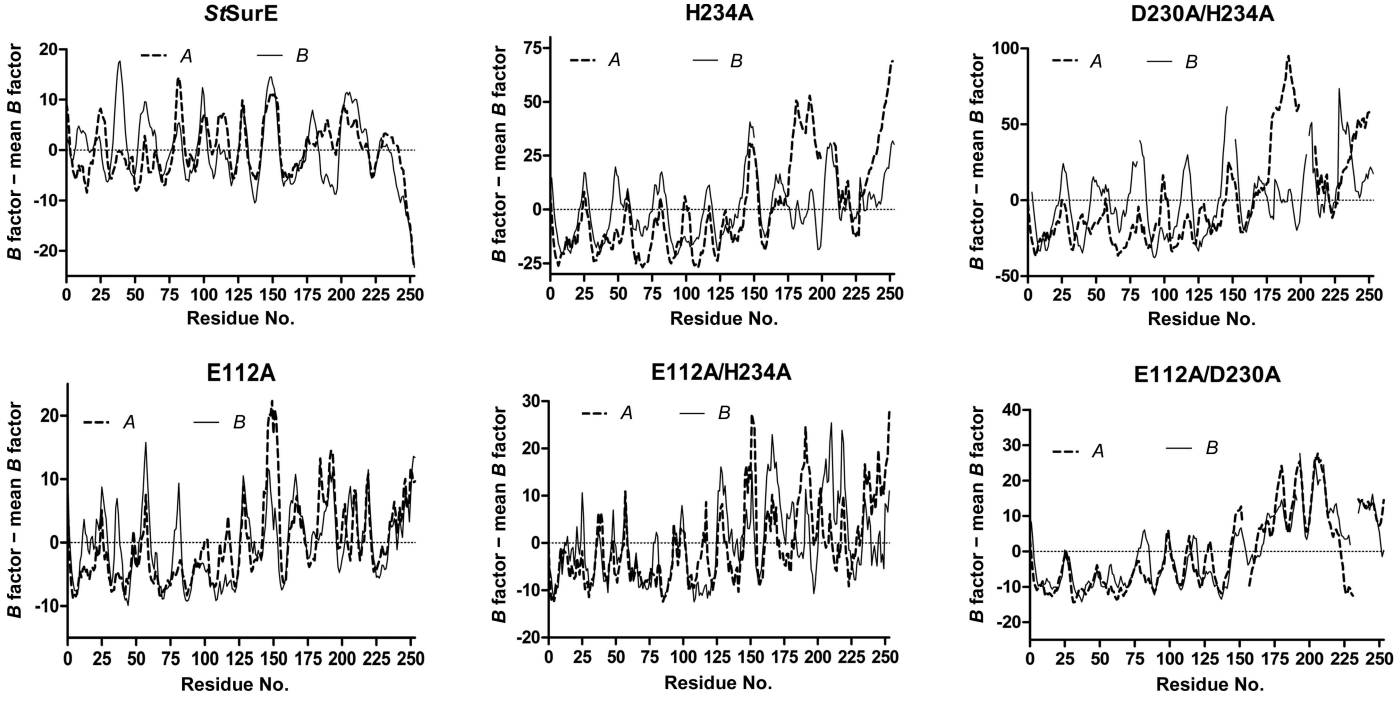

Figure 5
Deviation of the *B* factors of backbone atoms from the mean main-chain *B* factor of the respective chain *versus* residue number in native *St*SurE and the H234A, D230A/H234A, E112A, E112A/H234A and E112A/D230A mutants. Higher flexibility of the C-terminal domain (residues 125–253) is observed for the H234A, D230A/H234A and E112A/D230A mutants.

pocket' (Fig. 6). Thus, site 1 probably represents the substrate phosphate position during catalysis.

In the E112A mutant, there were two other positions with electron density suitable for a phosphate ion along a path that may represent the substrate-entry and product-release channel (Fig. 6). These sites were in the adenine pocket and at a site near residue 112. Some of the sites along this proposed channel were also found to bind ligands such as the cryoprotectants glycerol (native *St*SurE *C*2 and *F*222 forms, E112A mutant *C*2 form and E112A mutant soaked with AMP) or ethylene glycol (E112A/H234A mutant *F*222 form and E112A/H234A mutant form II), or ligands such as MPD (E112A mutant *C*2 form, E112A/H234A mutant *C*2 form and E112A/H234A mutant form I) or acetate ion (E112A/H234A mutant *C*2 form) that were part of the crystallization cocktail. The presence of these ligands/ions also supports the importance of the proposed channel for substrate entry/product release. Residues Asp8^{A}, Asp9^{A}, Ser39^{A}, Gly40^{A}, Asn92^{A}, Ala93^{A}, Gly94^{A}, Pro95^{A}, Asn96^{A}, Leu97^{A}, Asp99^{A}, Asp100^{A}, Tyr103^{A}, Ser104^{A}, Gly105^{A}, Thr106^{A}, Tyr128^{A}, Arg179^{A}, His180^{A}, Pro181^{A}, Ala182^{A}, Asp183^{A}, Ile199^{A}, Gly200^{A}, Pro202^{A}, Gly203^{A}, Phe214^{A}, Leu45^{B}, Leu47^{B}, Thr69^{B}, Tyr73^{B}, Val76^{B}, Asn77^{B}, Glu112^{B}, Gly113^{B}, Arg114^{B}, His115^{B} and Leu116^{B} are part of this proposed channel. The positively charged residues in this channel might guide the entry of the negatively charged substrate or promote product release. There are two such channels corresponding to the two protomers of the dimeric structure.

3.9. Role of loop 34–52 in *St*SurE

In *St*SurE, the loop consisting of residues 34–52 (Fig. 1*a*) is important for maintaining the active site in a conformation suitable for substrate binding (Pappachan *et al.*, 2008). Ser39 of this loop binds to the Mg^{2+} ion, and the main-chain N atom of Gly40 is hydrogen-bonded to the phosphate at site 1. In the H234A and D230A/H234A mutants, the C^{α} atom of Gly40 was displaced by ∼3.6 Å and the Asp8 side chain was distant from

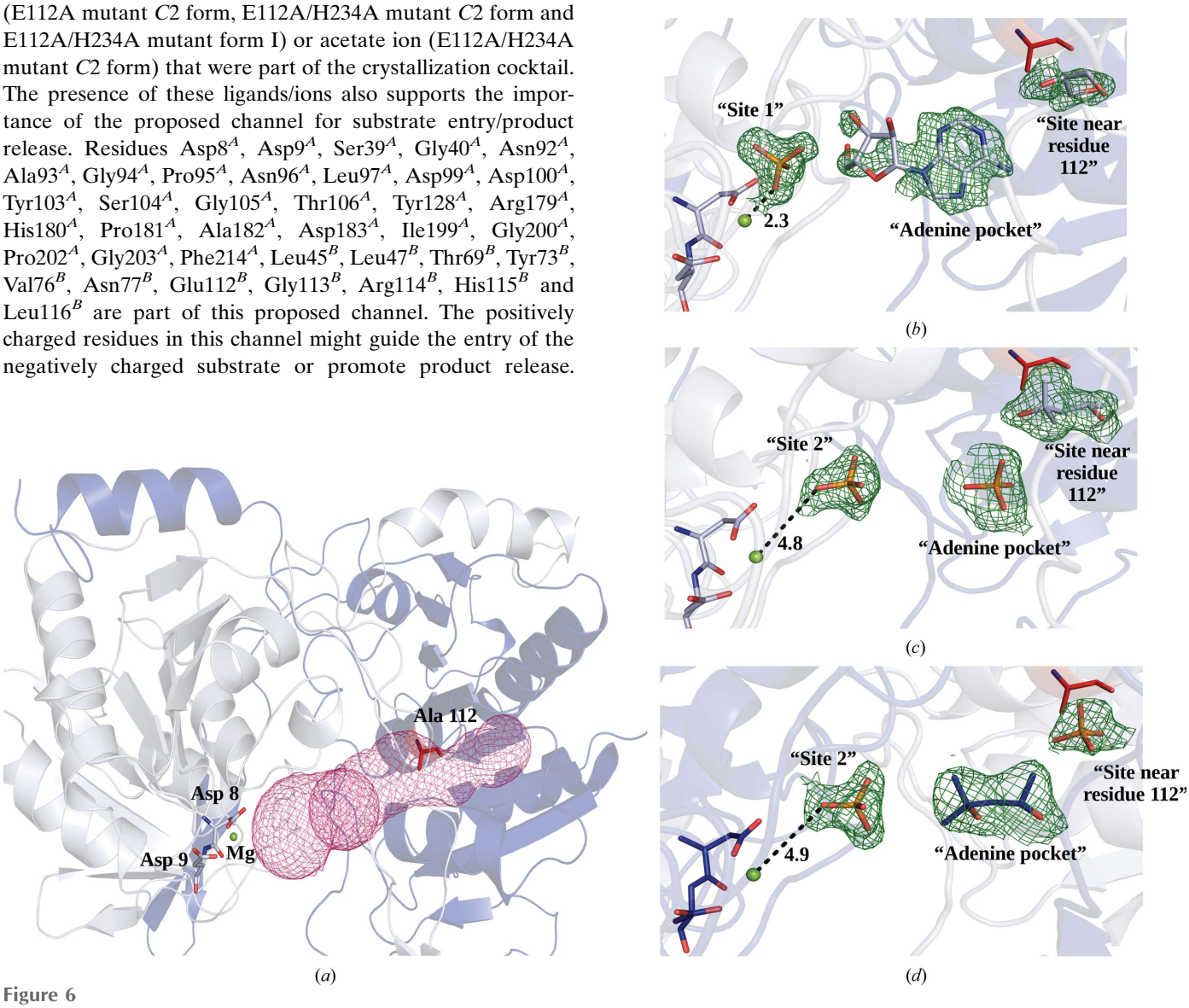

Figure 6
Substrate-entry/product-release channel inferred from the positions of bound phosphate ions and ligands. (*a*) The substrate-entry/product-release channel from the active site of chain *A* of the E112A mutant *A* (light blue)/*B* (dark blue) dimer is represented as a pink mesh (calculated using the *CAVER* plugin in *PyMOL*). The active-site residues Asp8 and Asp9 of chain *A* are shown in ball-and-stick representation and the Mg^{2+} ion is shown as a green sphere. The mutated residue 112 (red, ball-and-stick representation) is part of this channel. Simulated-annealing difference mapa ($F_o - F_c$, contoured at 2.9σ) of ligands bound in this channel are shown in (*b*), (*c*) and (*d*). (*b*) Chain *A* of the E112A mutant soaked with AMP (PDB entry 4xj7). A phosphate ion, an adenosine moiety and a glycerol molecule are bound at site 1, the adenine pocket and at a site near residue 112, respectively. (*c*) Chain *A* of the E112A mutant (PDB entry 4ryu). Two phosphate ions are bound at site 2 and the adenine pocket, while an MPD molecule is bound near residue 112. (*d*) Chain *B* of the E112A mutant (PDB entry 4ryu). Two phosphate ions are bound at site 2 and near residue 112, while a MPD molecule is bound at the adenine pocket. If residue 112 is modelled as a Glu, as in the native sequence, it will have a steric clash with phosphate/MPD/glycerol bound near it. Dstances are in Å.

the site of Mg^{2+} binding (Mathiharan *et al.*, 2013). Consequently, these mutants were found to be inactive. In these mutants the conformational change of this loop was largely influenced by the concerted movement of the swapped segments (Mathiharan *et al.*, 2013). Apart from maintaining the active-site conformation, the segment 39–45 of this loop from the *A* and *B* chains links the two active sites through a network of hydrogen bonds (Supplementary Table S2). In the H234A, D230A/H234A, E112A/H234A and E112A/D230A mutants there are changes in this hydrogen-bond network (Supplementary Table S2). These changes are owing to the alterations in the dimeric interface.

3.10. Conformational heterogeneity of the loop 34–52 in the E112A/H234A mutant

In the four structures of the E112A/H234A mutant obtained with or without soaking or co-crystallization with AMP, residues 39–40 could be built in two distinct conformations, in one of which the C^{α} atom of Ser39 is close (∼4 Å) to the Mg^{2+} ion as in the native structure. In the other conformation it is ∼6 Å away from the Mg^{2+} ion. These conformations may be considered as closed (4 Å) and open (6 Å) forms. In the closed conformation but not in the open conformation, the OH atom of Ser39 coordinates to the Mg^{2+} ion. In the unliganded *C*2 form of the E112A/H234A mutant (PDB entry 4xer), chains *A* and *D* are in the closed conformation (Fig. 7*a*), enabling interaction between Ser39 and the metal ion. However, in chains *B* and *C* the residues are in an open conformation and Ser39 is not close to the Mg^{2+} ion (Fig. 7*b*). The polypeptide backbone in the segment Ser39–Gly40 also shows significant displacement from its position in the native structure (Fig. 7*c*). In the *F*222 unliganded form of the E112A/H234A mutant (PDB entry 4xep) the polypeptide could be built in both conformations. Similar heterogeneity was observed with E112A/H234A mutant crystals obtained in the presence of AMP (chains *A*, *B* and *D* in the closed form and chain *C* in the the open form; PDB entry 4xgb) or soaked after crystallization in buffers containing AMP (chain *A* in the closed form and chains *B*, *C* and *D* in the open form; PDB entry 4xgp). This conformational heterogeneity might be owing to perturbations near residues Tyr103 and Ile102 caused by the E112A substitution, which eliminates the interaction of Glu112 with Tyr103, which along with Ile102 interacts with Ser42 of the loop 34–52 (Ile102 O–Ser42 OG, 2.7 Å; Tyr103 O–Ser42 N, 3.0 Å). This might account for the reduced phosphatase activity (74%) of the E112A/H234A mutant compared with the native protein.

Table 2
Kinetic parameters of *St*SurE mutants.

$[S]_{0.5} = (K')^{1/h}$, $K' = [S]_{0.5} = K_m$ when $h = 1$, $[S]_{0.5}$ is the substrate concentration when $V = V_{max}/2$, h is the Hill constant and K_m is the Michaelis–Menten constant.

	V_{max} (μmol min^{-1} mg^{-1})	K' (m*M*)	$[S]_{0.5}$ (m*M*)	*h*
Native	6.47 ± 0.04	5.83 ± 0.25	5.83	1
E112A	5.69 ± 0.13	2.23 ± 0.44	2.23	1
H234A	0.35 ± 0.04	81.00 ± 10.67	9.10	1.99
E112A/H234A	4.81 ± 0.27	5.29 ± 0.20	5.29	1
E112A/D230A	0.72 ± 0.06	71.88 ± 12.80	9.49	1.9
E112A/D230A/H234A	0.63 ± 0.17	63.07 ± 9.55	8.86	1.9

3.11. Functional studies on *St*SurE mutants

Alkaline phosphatase assays for the native and mutants were carried out as described in §2. The kinetic parameters obtained by monitoring the reaction at pH 7 and 25°C in the presence of Mg^{2+} ion are listed in Table 2. Michaelis–Menten kinetics were observed with native *St*SurE and the E112A and E112A/H234A mutants (Supplementary Figs. S4*a*, S4*b* and S4*c*). The V_{max} of the E112A mutant was comparable to that of the wild type. However, its K_m was significantly lower (Table 2). The Glu112 side chain is near the proposed substrate-entry channel and hence its negative charge might interfere with the entry of the negatively charged substrate. On the loss of the glutamate side chain, as evaluated by *CASTp* (Liang *et al.*, 1998*a*,*b*), the volume of the channel

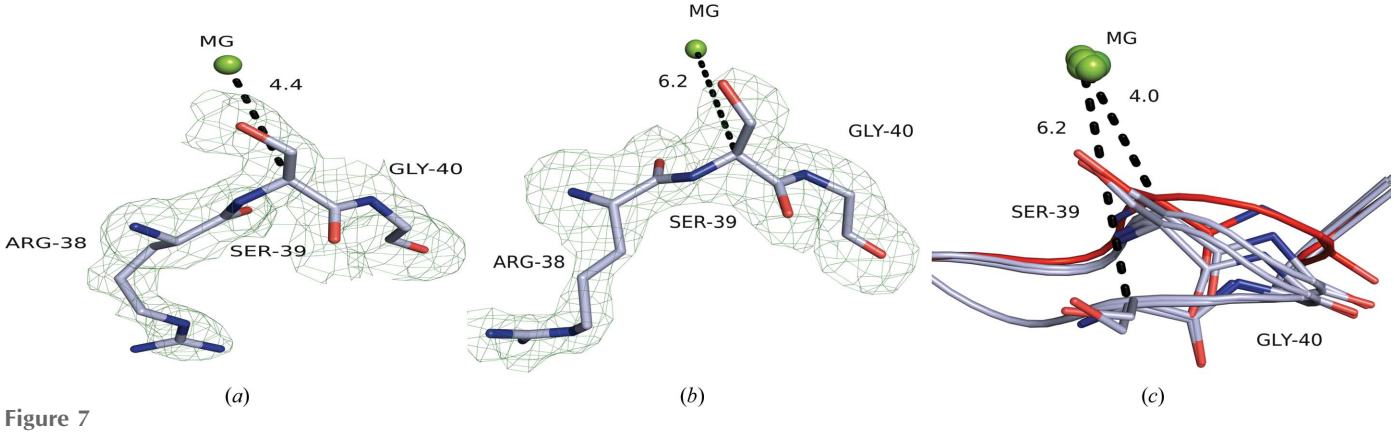

Figure 7
Conformational heterogeneity of the segment 39–40 near the active site in the E112A/H234A mutant. Fit of the segment 38–40 (ball-and-stick representation) to the difference electron-density map ($F_o - F_c$; calculated after omitting the segment 38–40; contoured at 2.8σ) in (*a*) the closed (chain *D*) and (*b*) the open (chain *B*) forms, respectively, of the *C*2 form of the E112A/H234A mutant (PDB entry 4xer). The metal ion in the active site is represented as a green sphere. Distances shown are in Å. (*c*) Comparison of the segment 39–40 in the four chains of the E112A/H234A mutant (PDB entry 4xer, light blue) with native *St*SurE (red). The change in the position of main-chain atoms can be noted.

increases from ∼1049 Å^3 in the native structure to ∼1275 Å^3 in the E112A mutant (*C*2 form). This increased volume and the concomitant reduced negative charge accounts for the reduction in the K_m of the E112A mutant.

The activity of the distorted mutant H234A was 5% of that of the native enzyme (Table 2). The curve could be fitted to a positive cooperativity model with a Hill coefficient of 1.99 (Supplementary Fig. S4*d*, Table 2). Similar cooperative behaviour has also been reported for some of the SurE homologues (Proudfoot *et al.*, 2004; Saraiva *et al.*, 2009). The $[S]_{0.5}$ values for native *St*SurE (5.83 m*M*) and the H234A mutant (9.10 m*M*) were comparable, although the activity was drastically reduced in the mutant (Table 2). The D230A and D230A/H234A mutants had no detectable activity even when high enzyme and substrate concentrations were used (data not shown). The drastic loss of activity in these mutants was probably owing to the change in the geometry of the active site (Mathiharan *et al.*, 2013).

In the E112A/H234A mutant the activity was mostly restored, and it follows Michaelis–Menten kinetics like the native enzyme. The activities of the E112A/D230A and E112A/D230A/H234A mutants were also restored (∼10% of that of the native enzyme); however, these mutants exhibited positive cooperativity (Supplementary Figs. S4*e* and S4*f*). The $[S]_{0.5}$ values of these mutants were comparable to that of the native (Table 2). These observations on the kinetic properties of active and inactive mutants and their structures suggest that the swapped, symmetric dimeric organization of the native protein is important for the function of *St*SurE.

4. Discussion

A large number of oligomeric proteins deposited in the PDB exhibit swapping of structural elements between protomers. Therefore, there is a need to experimentally address the structural features of domain swapping and its importance for oligomerization and function. In various proteins such as p13sucI (Rousseau *et al.*, 2001), CD2 (Murray *et al.*, 1998) and SgrAI (Park *et al.*, 2010), mutations in the hinge involved in swapping have been shown to affect oligomerization. In *St*SurE, loss of a crucial hydrogen bond in the hinge involved in C-terminal helix swapping was shown to affect the dimer organization and twofold symmetry of the dimer (Mathiharan *et al.*, 2013).

In this communication, the structural role of the new salt bridges (Glu112^A–Arg179^B and His180^A–Glu112^B) observed in the altered dimeric interface of the *St*SurE hinge mutants H234A and D230A/H234A were examined. From this viewpoint, additional mutations were introduced so as to eliminate the new salt bridges. Unexpectedly, the loss of the salt bridge in the double mutants E112A/H234A and E112A/D230A resulted in restoration of symmetry, and the dimers of these mutants closely resembled the wild-type dimers. This suggests that the distorted dimeric structure was indeed stabilized by the salt bridges Glu112^A–Arg179^B and His180^A–Glu112^B. Although the dimeric structure of the E112A/D230A mutant possesses nearly exact twofold symmetry, a residual rotation of 11° between the *B* chains was observed upon structural superposition of the *A* chains of the native and the E112A/D230A mutant structures. This result emphasizes how local stabilizing interactions play an important role in maintaining the tertiary and quaternary structures of proteins. In a wider context, this study demonstrates that loss of precise domain-swapping interactions is compensated by additional stabilizing interactions that preserve the oligomeric structure. This observation supports the previously suggested role of domain swapping in the evolution of oligomeric proteins (Ali & Imperiali, 2005).

Apart from oligomerization, domain swapping has been demonstrated to have additional roles such as the appearance of new binding sites (Shikamoto *et al.*, 2003; Mizuno *et al.*, 1999; Tegoni *et al.*, 1996), allosteric regulation of enzymes (Vitagliano *et al.*, 1999; Park *et al.*, 2010) and signal transduction in cell-cycle regulatory proteins (Bourne *et al.*, 1995). In *St*SurE also, domain-swapping interactions play an important role in catalysis. In the H234A and D230A/H234A mutants, changes in the swapped segments affected the conformation of the loop 34–52 and the geometry of the active site (Mathiharan *et al.*, 2013). As a consequence, the phosphatase activity was drastically reduced. In the salt-bridge mutants E112A/H234A and E112A/D230A, the restoration of the swapping interactions and dimeric organization also restored function. In the E112A/H234A mutant, although the dimeric structure was mostly preserved, there were alterations near residue 112 at the dimeric interface, leading to a dual conformation of the loop 34–52 (Fig. 7). As a consequence, the activity of the E112A/H234A mutant was reduced when compared with those of the native and the E112A mutant. The cooperativity observed in the H234A and E112A/D230A mutants might be a result of changes in the hydrogen-bonding network around loop 34–52 that links the active sites of two protomers. The increased flexibility of the C-terminal half in these mutants may also promote interaction between the two active sites. This emphasizes the significance of swapping interactions and symmetric dimeric organization for the function of *St*SurE.

The studies reported in this manuscript demonstrate the complexity and interplay of interactions that contribute to the precise oligomeric structure and catalytic function of proteins and the probable role of domain swapping in the evolution of symmetric protein oligomers. It would be of interest to understand whether these results could be generalized to other SurE homologues, as the C-terminal helix swapping and the crucial interactions stabilizing the hinge involved are mostly conserved.

Acknowledgements

The diffraction data were collected using the X-ray facility at the Molecular Biophysics Unit, Indian Institute of Science supported by the Department of Science and Technology (DST) and the Department of Biotechnology (DBT), Government of India and at ESRF Grenoble. We thank the staff of the X-ray laboratory at MBU and the beamline

scientists at BM14, ESRF for their cooperation during data collection. This project was supported by the Department of Science and Technology, the Department of Biotechnology, Government of India and by J. C. Bose fellowships to MRN and HSS. YKM was supported by CSIR, India.

References

Ali, M. H. & Imperiali, B. (2005). *Bioorg. Med. Chem.* **13**, 5013–5020.

Antonyuk, S. V., Ellis, M. J., Strange, R. W., Bessho, Y., Kuramitsu, S., Shinkai, A., Yokoyama, S. & Hasnain, S. S. (2009). *Acta Cryst.* F**65**, 1204–1208.

Bourne, Y., Arvai, A. S., Bernstein, S. L., Watson, M. H., Reed, S. I., Endicott, J. E., Noble, M. E. M., Johnson, L. N. & Tainer, J. A. (1995). *Proc. Natl Acad. Sci. USA*, **92**, 10232–10236.

Cohen, G. H. (1997). *J. Appl. Cryst.* **30**, 1160–1161.

Emsley, P., Lohkamp, B., Scott, W. G. & Cowtan, K. (2010). *Acta Cryst.* D**66**, 486–501.

Franklin, M. C., Cheung, J., Rudolph, M. J., Burshteyn, F., Cassidy, M., Gary, E., Hillerich, B., Yao, Z.-K., Carlier, P. R., Totrov, M. & Love, J. D. (2015). *Proteins*, doi:10.1002/prot.24841.

Iwasaki, W. & Miki, K. (2007). *J. Mol. Biol.* **371**, 123–136.

Krissinel, E. & Henrick, K. (2004). *Acta Cryst.* D**60**, 2256–2268.

Laskowski, R. A., MacArthur, M. W., Moss, D. S. & Thornton, J. M. (1993). *J. Appl. Cryst.* **26**, 283–291.

Lee, J. Y., Kwak, J. E., Moon, J., Eom, S. H., Liong, E. C., Pedelacq, J.-D., Berendzen, J. & Suh, S. W. (2001). *Nature Struct. Biol.* **8**, 789–794.

Liang, J., Edelsbrunner, H., Fu, P., Sudhakar, P. V. & Subramaniam, S. (1998*a*). *Proteins*, **33**, 1–17.

Liang, J., Edelsbrunner, H., Fu, P., Sudhakar, P. V. & Subramaniam, S. (1998*b*). *Proteins*, **33**, 18–29.

Mathiharan, Y. K., Pappachan, A., Savithri, H. S. & Murthy, M. R. N. (2013). *PLoS One*, **8**, e55978.

McCoy, A. J., Grosse-Kunstleve, R. W., Adams, P. D., Winn, M. D., Storoni, L. C. & Read, R. J. (2007). *J. Appl. Cryst.* **40**, 658–674.

Mizuno, H., Fujimoto, Z., Koizumi, M., Kano, H., Atoda, H. & Morita, T. (1999). *J. Mol. Biol.* **289**, 103–112.

Mura, C., Katz, J. E., Clarke, S. G. & Eisenberg, D. (2003). *J. Mol. Biol.* **326**, 1559–1575.

Murray, A. J., Head, J. G., Barker, J. J. & Brady, R. L. (1998). *Nature Struct. Mol. Biol.* **5**, 778–782.

Murshudov, G. N., Skubák, P., Lebedev, A. A., Pannu, N. S., Steiner, R. A., Nicholls, R. A., Winn, M. D., Long, F. & Vagin, A. A. (2011). *Acta Cryst.* D**67**, 355–367.

Pappachan, A., Savithri, H. S. & Murthy, M. R. N. (2008). *FEBS J.* **275**, 5855–5864.

Park, C. K., Joshi, H. K., Agrawal, A., Ghare, M. I., Little, E. J., Dunten, P. W., Bitinaite, J. & Horton, N. C. (2010). *PLoS Biol.* **8**, e1000554.

Proudfoot, M., Kuznetsova, E., Brown, G., Rao, N. N., Kitagawa, M., Mori, H., Savchenko, A. & Yakunin, A. F. (2004). *J. Biol. Chem.* **279**, 54687–54694.

Rousseau, F., Schymkowitz, J. W., Wilkinson, H. R. & Itzhaki, L. S. (2001). *Proc. Natl Acad. Sci. USA*, **98**, 5596–5601.

Saraiva, A. M., Reis, M. A., Tada, S. F., Rosselli-Murai, L. K., Schneider, D. R. S., Pelloso, A. C., Toledo, M. A. S., Giles, C., Aparicio, R. & de Souza, A. P. (2009). *FEBS J.* **276**, 6751–6762.

Shikamoto, Y., Morita, T., Fujimoto, Z. & Mizuno, H. (2003). *J. Biol. Chem.* **278**, 24090–24094.

Tegoni, M., Ramoni, R., Bignetti, E., Spinelli, S. & Cambillau, C. (1996). *Nature Struct. Mol. Biol.* **3**, 863–867.

Vitagliano, L., Adinolfi, S., Sica, F., Merlino, A., Zagari, A. & Mazzarella, L. (1999). *J. Mol. Biol.* **293**, 569–577.

Winn, M. D. *et al.* (2011). *Acta Cryst.* D**67**, 235–242.

Zhang, R. G., Skarina, T., Katz, J. E., Beasley, S., Khachatryan, A., Vyas, S., Arrowsmith, C. H., Clarke, S., Edwards, A., Joachimiak, A. & Savchenko, A. (2001). *Structure*, **9**, 1095–1106.